Evaluating the performance of robust controllers for a nanopositioning platform under loading.

Douglas Russell and Sumeet S. Aphale

*Centre for Applied Dynamics Research, School of Engineering,
King's College, University of Aberdeen, UK,
(email: r01dr12@abdn.ac.uk and s.aphale@abdn.ac.uk)*

Abstract: Piezoactuated nanopositioners are an integral component in Scanning Probe Microscopes (SPM). The imaging application of SPMs necessitate the loading of the nanopositioning platform with various samples. This causes an increase in mass thereby altering the dynamics of the system. Various methods have been proposed to control uncertain systems such as $\mathcal{H}_\infty$ robust control, μ-synthesis and mixed μ-synthesis. Additionally, low-order damping controllers, such as Integral Resonance Control (IRC) and Positive Position Feedback (PPF), have been shown to be robustly stable via the negative imaginary lemma. In this paper, IRC is used as a benchmark for robust performance, and robust controllers are developed using the aforementioned methods. It is found that the best performance, in terms of the $\mathcal{H}_\infty$ norm over the range of uncertainty, is achieved using the IRC control scheme. In addition, IRC provides more accurate tracking of a reference signal.

Keywords: Vibration control, Micro and Nano Mechatronic Systems, Modeling.

1. INTRODUCTION

The use of piezoelectric stack-actuated nanopositioning platforms in scanning probe microscopy presents a challenge in robust control under uncertainty due to loading. By modelling a nanopositioning platform as a mass-spring-damper system [Fleming (2010)], it can be seen that loading a sample onto the platform increases the mass of the platform, thereby altering the system dynamics, e.g. a reduction of the resonance frequency. Typical open-loop control methods, such as model-based inversion [Croft et al. (2001)], are not applicable as these require a highly accurate model of the system which cannot be obtained due to the variability of the mass. This necessitates the use of closed-loop control techniques in order to achieve accurate positioning in uncertain systems. Two methods are considered: robust control, and the combination of damping and tracking controllers.

Robust control uses optimisation techniques, such as $\mathcal{H}_\infty$ and μ-synthesis, to develop high-performing controllers by minimising a cost function which defines the performance objectives. Successful implementation of $\mathcal{H}_\infty$ robust control in nanopositioning applications has been reported in the literature [Salapaka et al. (2002); Sebastian and Salapaka (2005); Sebastian et al. (2008)]. Whilst the authors are unaware of any application of μ-synthesis in nanopositioning, it has found use in comparable systems. Moser (1993) shows an implementation of μ-synthesis control in flexible structures, and Tayebi et al. (2008) presents an application in robotic manipulators. These applications are examples of collocated systems, for which the same control methods can be utilised [Aphale et al. (2007); Pereira et al. (2011)]. This suggests that the use of μ-synthesis in nanopositioning applications is feasible.

Another prevalent method for the control of nanopositioning systems is the use of damping controllers, such as Integral Force Feedback (IFF) [Preumont et al. (2008)], Integral Res-

onance Control (IRC) [Aphale et al. (2008b)], Positive Position Feedback (PPF) [Fanson and Caughey (1990)], Positive Velocity and Position Feedback (PVPF, also known as Polynomial Based Control) [Bhikkaji et al. (2007)] and Resonant Control [Aphale et al. (2008a)], in conjunction with an integral tracking controller in an external feedback loop. It has been shown that IRC, PPF, and Resonant Control are strictly negative-imaginary (SNI). For a nanopositioning system with collocated sensor actuator pairs, these controllers provide robust stability via the negative-imaginary lemma [Peterson and Lanzon (2010)]. In addition, the use of controllers with integral action has been shown to provide a significant reduction in the effects of inherent nonlinear behaviours such as hysteresis and creep [Devasia et al. (2007)].

In this work, IRC is used as a benchmark to design robust controllers using $\mathcal{H}_\infty$, μ-synthesis, and mixed μ-synthesis optimisation techniques. This is achieved by choosing weighting functions which act as upper bounds on the functions measured from the reference to the regulated outputs, in this case, the error, sensor output, and control signal. Using these weighting functions provides a simple measure of improved performance, that is, the robust controller provides improved performance over IRC if the $\mathcal{H}_\infty$ norm of the regulated system is less than that of IRC. IRC is chosen as it provides robust stability, has low order and a simple design procedure.

The paper is structured as follows: Section 2 develops a model of the system with variable mass. The method of controller design for both IRC and the three robust controllers is described in Section 3. Section 4 provides an overview of the experimental system upon which the models are based and the derivation of the plant model. In this section, simulated and experimental results in both the frequency and time domain are presented. The performance of each control scheme is analysed in both the nominal- and worst-case to evaluate the effect of a change
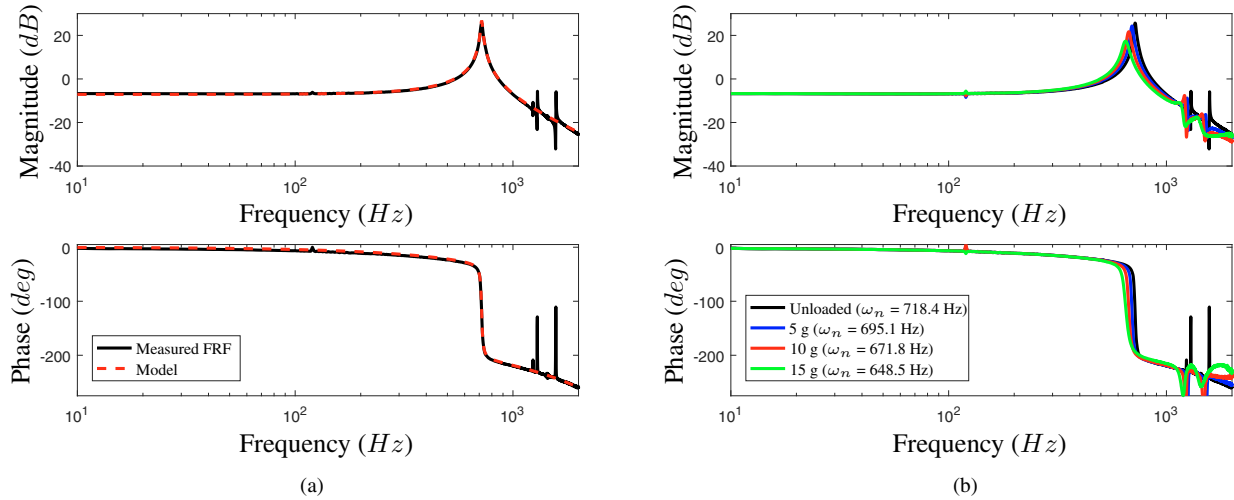
Fig. 1. (a) Measured frequency response and model of the nominal system, and (b) Measured frequency response of the system under loading.

in mass on closed-loop performance. Section 5 concludes the paper.

2. SYSTEM MODELLING

A single axis of a nanopositioning platform can be modelled as a mass-spring-damper system, having equation of motion

$$M_p \ddot{d} + c_f \dot{d} + kd = F_a, \qquad (1)$$

where M_p is the mass of the platform, c_f is the damping coefficient of the flexures, k is the sum of the spring stiffness of the flexures, k_f, and the actuator, k_a, and F_a is the force applied by the actuator.

Taking the Laplace transform of the equation of motion, the transfer function measured from the applied force, F_a, to the displacement, d, is

$$G_{dF_a}(s) = \frac{d}{F_a} = \frac{1}{M_p s^2 + c_f s + k}. \qquad (2)$$

The force generated by the actuator can be related to the unconstrained piezoelectric expansion, δ, by

$$F_a = k_a \delta, \qquad (3)$$

and δ can be related to the reference input voltage, r, by

$$\delta = g_{\delta r} r = d_{33} n g_a r, \qquad (4)$$

where $g_{\delta r}$ is a constant gain which is the product of the piezoelectric strain constant, d_{33}, the number of actuator layers, n, and the amplifier gain, g_a.

Likewise, the displacement, d, can be related to the measured voltage, y, by

$$d = g_s y, \qquad (5)$$

where g_s is the sensor gain. The transfer function from the reference input, r, to the measured voltage, y, is then

$$
G_p(s) = \frac{y}{r} = \frac{\frac{k_a g_{\delta r}}{g_s}}{M_p s^2 + c_f s + k}
$$
$$
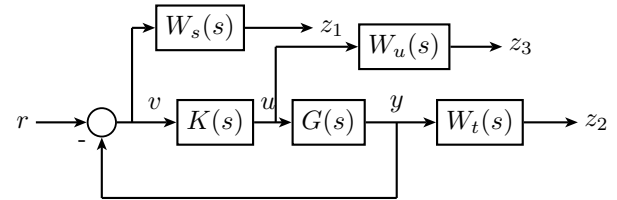= \frac{\frac{g}{M_p}}{s^2 + \frac{c_f}{M_p}s + \frac{k}{M_p}}, \qquad (6)
$$

Fig. 2. Block diagram of the closed-loop system with regulated outputs.

where $g = k_a g_{\delta r}/g_s$, or substituting standard variables

$$G_p(s) = \frac{\sigma^2}{s^2 + 2\zeta_p \omega_p s + \omega_p^2}. \qquad (7)$$

It is known from experimentally measured results that nanopositioning platforms have multiple resonance modes. However, the behaviour of nanopositioners is dominated by a single low frequency resonance mode, and so, it is not necessary to model any higher-order modes.

In addition to the plant dynamics, the amplifier and sensor affect the measured response and can be modelled as first-order low pass filters, i.e.

$$H_s(s) = \frac{\omega_s}{s + \omega_s}, H_a(s) = \frac{\omega_a}{s + \omega_a}. \qquad (8)$$

A small time-delay is also observed in the experimentally measured frequency response due to hardware/software latency, and is modelled as a second-order pade approximation, as in [San-Millan et al. (2015)], giving

$$D(s) = \frac{s^2 - as + b}{s^2 + as + b}. \qquad (9)$$

The full model of the plant is then given by:

$$G(s) = H_s(s)D(s)G_p(s)H_a(s). \qquad (10)$$

3. CONTROLLER DESIGN

It is desired that the closed-loop system provide low error at low frequencies, high roll-off at high frequencies (to reduce the effects of noise), and bounded control signal (to prevent
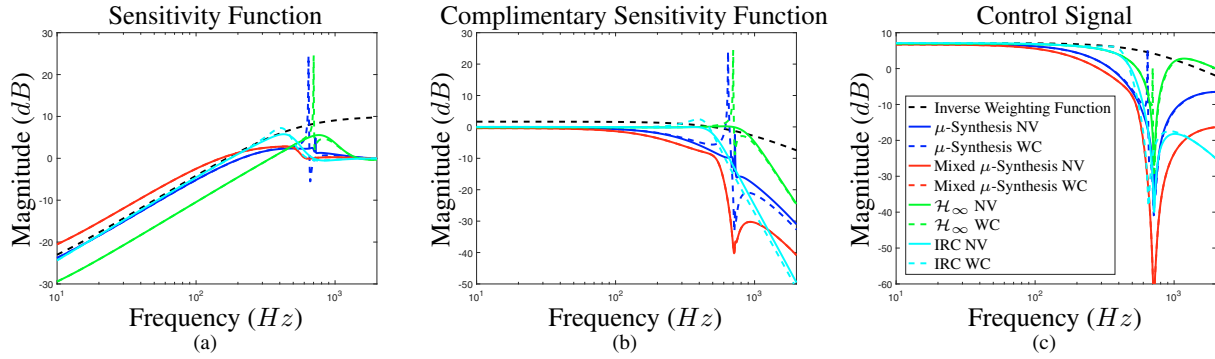
Fig. 3. The (a) sensitivity function, (b) complimentary sensitivity function, and (c) function measured from the reference to the control signal, showing both the nominal and worst-case responses.

saturation). This is achieved by regulating the relevant outputs as shown in Fig. 2.

One method of ensuring low errors at low frequencies and high roll-off at high frequencies is the use of damping and tracking controllers. In this work, we consider IRC. IRC is chosen as it is known to be robustly stable via the negative imaginary lemma and is used as a benchmark of robust performance.

The IRC control scheme consists of a first order damping controller, $C_d(s)$, in positive feedback, and an integral tracking controller, $C_t(s)$, implemented in negative feedback, given by

$$C_d(s) = \frac{k}{s - dk}, C_t(s) = \frac{k_t}{s}. \quad (11)$$

As the damping controller is SNI, the inner damping loop is robustly stable if

$$|G(j0)C_d(j0)| < 1. \quad (12)$$

This inequality holds if

$$d < -\frac{\sigma^2}{\omega_p^2} = -d_c. \quad (13)$$

The feedthrough term, d, is chosen to be $d = -2d_c$, as in [Namavar et al. (2014)], which ensures unity DC gain in the damping loop as well as robust stability. The damping gain, k, is chosen using root locus analysis to ensure the greatest achievable damping. The tracking gain, k_t, is chosen as the largest value such that the closed-loop magnitude response does not exceed unity gain.

The robust control problem is formulated to minimise the error at low frequencies, maximise the roll-off at high frequencies, and bound the control signal. The cost function is defined as

$$\left\| \begin{matrix} W_s S \\ W_t T \\ W_u U \end{matrix} \right\|_\infty < \gamma/\mu \quad (14)$$

where S is the sensitivity function, T is the complimentary sensitivity function, and U is the function measured from the input to the control signal. The plant, shown in Fig. 2, is then defined as

$$P = \begin{bmatrix} z_1 \\ z_2 \\ z_3 \\ v \end{bmatrix} = \begin{bmatrix} W_s & -W_s G \\ 0 & W_t G \\ 0 & W_u \\ 1 & -G \end{bmatrix} \begin{bmatrix} r \\ u \end{bmatrix}. \quad (15)$$

The weighting functions, W_s, W_t and W_u, are chosen such that their inverse acts as an upper bound of the corresponding function of the IRC design, i.e.

$$\|W_s S_{IRC}\|_\infty = \|W_t T_{IRC}\|_\infty = \|W_u U_{IRC}\|_\infty = 1. \quad (16)$$
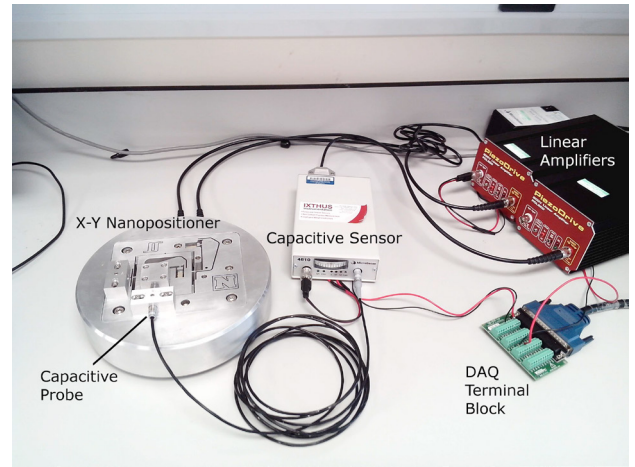

Fig. 4. A two-axis serial-kinematic nanopositioning platform designed and constructed by EasyLab, University of Nevada, Reno, USA.

It follows that the robust controller provides improved performance over IRC if

$$\left\| \begin{matrix} W_s S \\ W_t T \\ W_u U \end{matrix} \right\|_\infty < \left\| \begin{matrix} W_s S_{IRC} \\ W_t T_{IRC} \\ W_u U_{IRC} \end{matrix} \right\|_\infty \quad (17)$$

over the range of the uncertainty, M. In the following section three methods, $\mathcal{H}_\infty$, μ-synthesis and mixed μ-synthesis, are used to develop robust controllers which minimise the cost function.

4. RESULTS AND DISCUSSION

4.1 Experimental Setup

Simulations are performed using models of a two-axis piezo-electric stack-actuated serial-kinematic long-range nanopositioning platform designed and constructed by EasyLab, University of Nevada, Reno, USA, pictured in Fig. 4. This provides a range of approximately 43 μm on each axis corresponding to an applied voltage of 0-200 V. Each axis is driven by a Piezodrive PDL200 linear voltage amplifier with a gain of 20, and bias of 100 V. The displacement is measured using a Microsense 4810 capacitive displacement sensor and a 2805 measurement probe providing a range of ± 50 μm or ± 10 V.
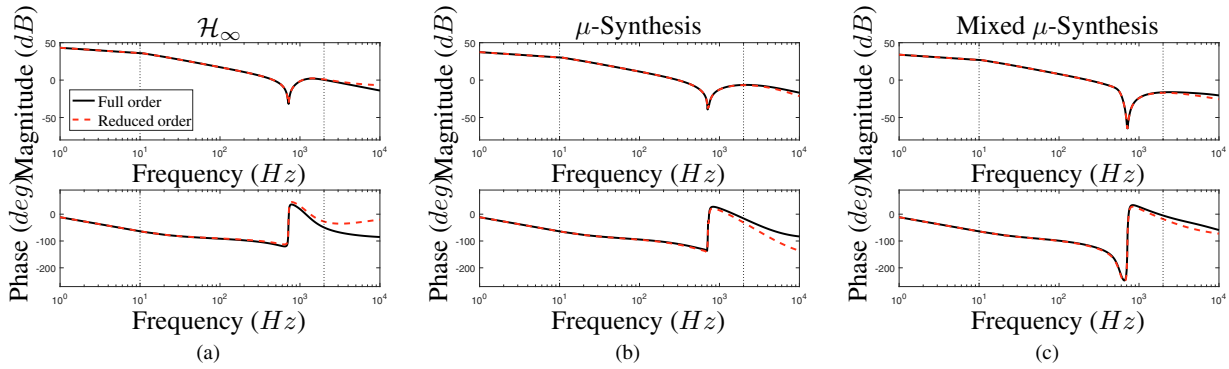
Fig. 5. Frequency response of the full- and reduced-order controllers. The reduced-order models deviate from the full-order model at high frequencies but are consistent within the bandwidth of interest, depicted by the dotted ($\cdots$) lines.

Table 1. Controller Performance

	Full Order			Reduced Order		
	γ/μ	Worst-case gain	Order	γ/μ	Worst-case gain	Order
IRC	1.6045	1.9603	2	1.6045	1.9603	2
$\mathcal{H}_\infty$	1.3618	28.463	22	1.8251	21.8045	10
μ-Synthesis	1.5568	20.1112	68	1.5569	8.0849	9
Mixed μ-Synthesis	1.8281	1.8281	58	1.8233	1.8233	9

4.2 System Identification

The nominal model of the platform dynamics is found via trial and error. Both the sensor and amplifier are modelled as first-order low pass filters with a cutoff frequency of 10000 Hz and 5000 Hz respectively. A time-delay of 65 μs is identified, due to hardware/software latency, giving:

$$G(s) = \frac{1.777 \times 10^{16} s^2 - 1.64 \times 10^{21} s + 5.046 \times 10^{25}}{\begin{array}{c} s^6 + 1.866 \times 10^5 s^5 + 1.355 \times 10^{10} s^4 \\ + 4.549 \times 10^{14} s^3 + 5.922 \times 10^{18} s^2 \\ + 9.673 \times 10^{21} s + 1.142 \times 10^{26} \end{array}}$$

(18)

as the nominal model. Fig. 1 shows the effect of the addition of mass in 5 g increments. Each additional 5 g mass causes a decrease in the resonance frequency of approximately 23.3 Hz. From this the physical parameters are found as:

$$M_p = 73.36g$$
$$k = 1.49 \times 10^6 Nm^{-1}$$
$$c_f = 6.62 Nsm^{-1}$$
$$g = 6.60 \times 10^5.$$

(19)

The frequency response of the nominal and perturbed models are given in Fig. 1. It is observed that the perturbed model more accurately matches the measured data when c_f/M_p is kept constant. The model of the plant dynamics is then defined as:

$$G_p(s) = \frac{\frac{g}{M} e^{-115 \times 10^{-6} s}}{s^2 + \frac{c_f}{M_{nom}} s + \frac{k}{M}}$$

(20)

where M_{nom} is the nominal mass, and M is an uncertain parameter with a range of 73.36 to 88.36 g.

4.3 Controller Design

The IRC damping controller is designed to maximise damping as in Namavar et al. (2014). The tracking controller is an integrator with the gain chosen such that the magnitude response does not exceed unity gain. The weighting functions which bound the IRC response are defined as:

$$W_s = 0.315 \times \frac{s + 3160}{s + 31.6}$$
$$W_t = 8.25 \times \frac{s + 4500}{s + 45000}$$
$$W_u = 4.41 \times \frac{s + 4500}{s + 45000}.$$

(21)

Three methods are used to develop a robust controller for the uncertain plant: μ-synthesis, mixed μ-synthesis, and $\mathcal{H}_\infty$, using the Matlab functions `dksyn` and `hinfsyn` respectively.

4.4 Simulated Results

The sensitivity function, complimentary sensitivity function, and function measured from the reference input, $r(t)$ to the control signal, $u(t)$, are plotted in Fig. 3 and the robust performance metrics are given in Table 1, where γ/μ is the $\mathcal{H}_\infty$ norm of the nominal system, and the worst-case gain is the largest $\mathcal{H}_\infty$ norm of the perturbed system. It is observed that, in the nominal case, the greatest performance is obtained using the $\mathcal{H}_\infty$ controller. However, the worst-case analysis shows that IRC provides improved performance over the range of uncertain mass. Both the $\mathcal{H}_\infty$ and μ-synthesis controllers perform poorly as the mass of the platform changes. This is seen as spikes in the sensitivity and complimentary sensitivity functions. For the mixed μ-synthesis controller, the worst-case is the nominal case, and so, the performance is not worsened by an increase in mass. It is noted that the mixed μ-synthesis provides the worst performance in the nominal case.

4.5 Experimental results

To verify the performance of the robust controllers, experiments were performed using the system described in Section 4.1. Reduced order controllers are used due to the limitation of system bandwidth and to simplify implementation. The controller order reduction is achieved by removing the poles and zeros which occur above 5000 Hz, and the pole/zero cancellations. The robust performance metrics for the reduced order controllers are given in Table 1 and the frequency responses are
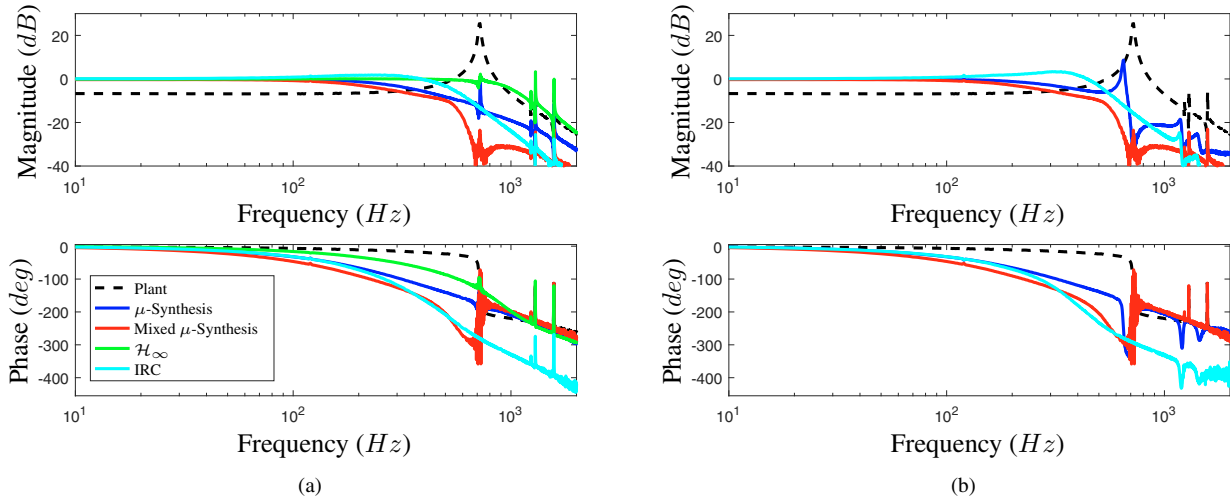
Fig. 6. Experimentally measured closed-loop frequency response of the (a) nominal, and (b) worst-case uncertainty. The worst-case $\mathcal{H}_\infty$ response is not presented as the additional mass which causes instability is less than that which causes the theoretical worst-case.

Table 2. Experimental Results

	Bandwidth (Hz)		RMS Error (nm)			
	Nominal	Worst-case	0g	5g	10g	15g
IRC	490	496	11.197	10.981	11.224	11.106
$\mathcal{H}_\infty$	916	unstable	20.431	unstable	unstable	unstable
μ-synthesis	286	304	13.456	13.441	13.507	13.491
Mixed μ-synthesis	204	204	20.405	20.370	20.412	20.404

plotted in Fig. 5. It is observed that, although the reduced order controllers differ from the full order at high frequencies, the response is consistent within the bandwidth of interest. Additionally, the use of reduced order controllers does not significantly reduce the performance in the nominal case and improves the worst-case performance for each of the three robust controllers.

The closed-loop frequency response for each of the robust control schemes is plotted in Fig. 6, and the bandwidth for both the nominal and worst-case given in Table 2. Whilst the $\mathcal{H}_\infty$ control scheme provides the greatest bandwidth in the nominal case, it is found that it becomes unstable for an additional mass greater than 2.06 g. This is less than the mass which causes the theoretical worst-case (2.29 g) and so cannot be included in Fig. 6(b). The μ-synthesis scheme develops a resonance peak as the mass is increased but remains stable. The worst-case mixed μ-synthesis is the nominal case and so performance is not degraded by an increase in mass. The bandwidth of IRC, μ-synthesis and mixed μ-synthesis is consistent over the range of uncertainty.

The response of the unloaded and loaded system to a 20 Hz triangle wave is shown in Fig. 7 and the corresponding RMS error given in Table 2. With the exception of $\mathcal{H}_\infty$ due to instability, the tracking accuracy of the three remaining control schemes is not significantly altered by an increase in mass. It can be seen that IRC provides the lowest tracking error, in terms of both the maximum and rms error, for the range of uncertain mass. In the case of μ-synthesis, small oscillations can be observed in the error signal, becoming more prominent as the mass is increased. This is consistent with the development of a resonance peak, shown in Fig. 6, and is predicted by simulation.

5. CONCLUSION

Imaging applications of nanopositioning platforms require robustness against perturbations of the system dynamics due to loading of the platform. Traditionally, robust control has favoured optimisation techniques such as $\mathcal{H}_\infty$ and μ-synthesis. Recent work on negative imaginary control has shown the robust stability of low-order controllers, such as IRC, for collocated systems. From this paper, the following conclusions can be drawn:

(1) $\mathcal{H}_\infty$ provides the greatest theoretical performance in the nominal case but small increases in mass cause instability in practice.
(2) μ-synthesis gives robust stability but an increase in mass induces oscillations in the system response.
(3) In terms of the $\mathcal{H}_\infty$ norm, mixed μ-synthesis shows the greatest performance over the full range of uncertainty. In practice, it provides the smallest bandwidth and largest tracking error of the controllers considered.
(4) IRC has a simple design procedure, low order, and does not necessitate model order reduction for implementation. In addition, IRC shows stability and the greatest tracking accuracy over the range of additional mass.

REFERENCES

Aphale, S.S., Bhikkaji, B., and Moheimani, S.R. (2008a). Minimizing scanning errors in piezoelectric stack-actuated nanopositioning platforms. *IEEE Transactions on Nanotechnology*, 7(1), 79–90.

Aphale, S.S., Fleming, A.J., and Moheimani, S.O.R. (2007). Integral resonant control of collocated smart structures. *Smart Materials and Structures*, 16, 439 – 446.
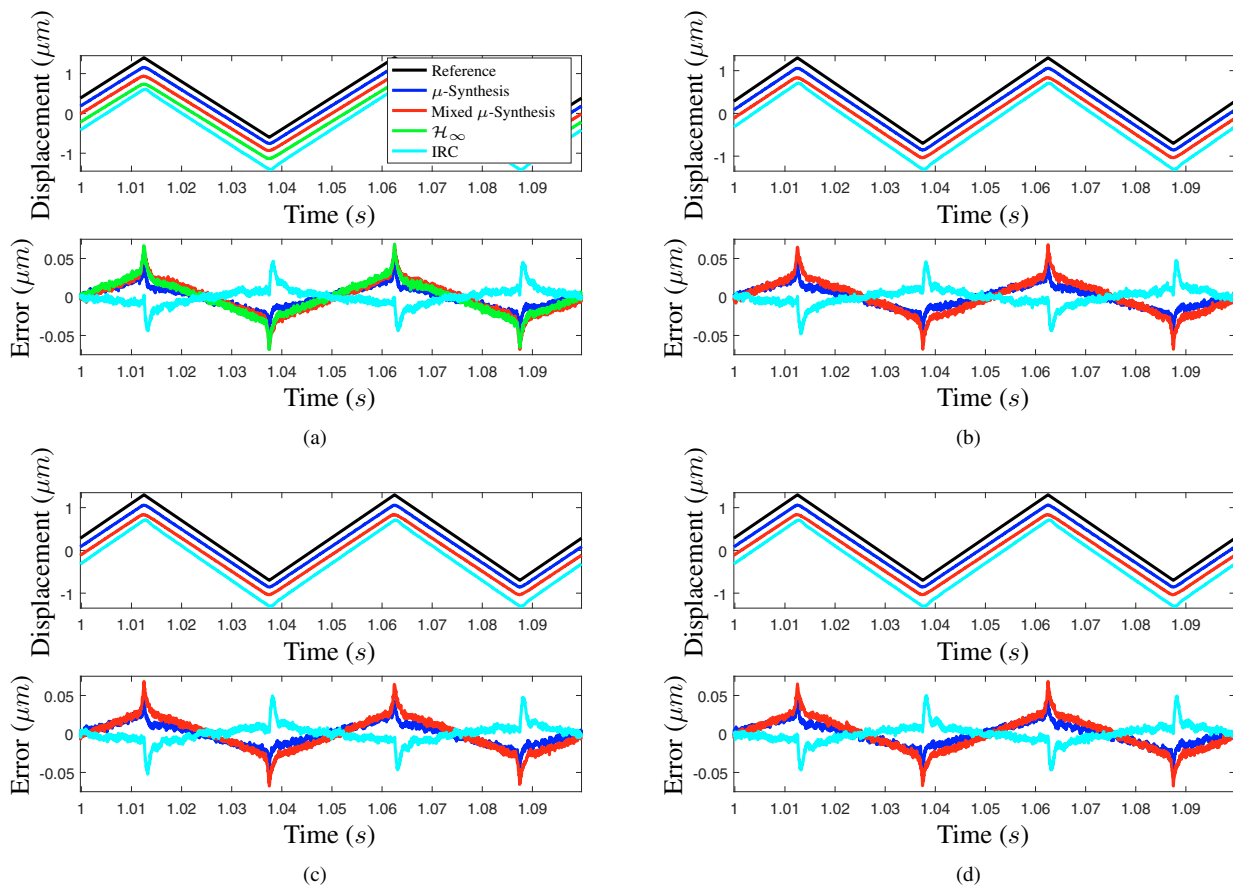
Fig. 7. Experimentally measured closed-loop response to a 20 Hz triangle wave for the (a) unloaded system, and with an additional mass of (b) 5 g, (c) 10 g, and (d) 15 g.

Aphale, S.S., Fleming, A.J., and Moheimani, S.O.R. (2008b). A second-order controller for resonance damping and tracking control of nanopositioning systems. In *19th International Conference on Adaptive Structures and Technologies, Ascona, Switzerland, October 6-9*.

Bhikkaji, B., Ratnam, M., Fleming, A.J., and Moheimani, S.O.R. (2007). High-performance control of piezoelectric tube scanners. *IEEE Transactions on Control Systems Technology*, 15(5), 853 – 866.

Croft, D., Shed, G., and Devasia, S. (2001). Creep, hysteresis, and vibration compensation for piezoactuators: Atomic force microscopy application. *Journal of Dynamic Systems, Measurement, and Control*, 123, 35–43.

Devasia, S., Eleftheriou, E., and Moheimani, S.O.R. (2007). A survey of control issues in nanopositioning. *IEEE Transactions on Control Systems Technology*, 15(4), 689 – 703.

Fanson, J.L. and Caughey, T.K. (1990). Positive position feedback control for large space structures. *AIAA Journal*, 28(4), 717 – 724.

Fleming, A.J. (2010). Nanopositioning system with force feedback for high-performance tracking and vibration control. *IEEE / ASME Transactions on Mechatronics*, 15(3), 433–447.

Moser, A.N. (1993). Designing controllers for flexible structures with h-infinity/ mu -synthesis. *IEEE Control Systems*, 13(2), 79–89.

Namavar, M., Fleming, A.J., Aleyaasin, M., Nakkeeran, K., and Aphale, S.S. (2014). An analytical approach to integral resonant control of second-order systems. *IEEE Transactions on Mechatronics*, 19(2), 651–659.

Pereira, E., Aphale, S.S., Feliu, V., and Moheimani, S.O.R. (2011). Integral resonant control for vibration damping and precise tip-positioning of a single-link flexible manipulator. *IEEE / ASME Transactions on Mechatronics*, 16(2), 232 – 240.

Peterson, I.R. and Lanzon, A. (2010). Feedback control of negative-imaginary systems. *IEEE Control Systems Magazine*, 54 – 72.

Preumont, A., de Marneffe, B., Deraemaeker, A., and Bossens, F. (2008). The damping of a truss structure with a piezoelectric transducer. *Computers and Structures*, 86, 227 – 239.

Salapaka, S., Sebastian, A., Clevland, J.P., and Salapaka, M.V. (2002). High bandwidth nano-positioner: A robust control approach. *Review of Scientific Instruments*, 73(9), 3232 – 3241.

San-Millan, A., Russell, D., Feliu, V., and Aphale, S.S. (2015). A modified positive velocity and position feedback scheme with delay compensation for improved nanopositioning performance. *Smart Materials and Structures*, 24(7), 075021.

Sebastian, A., Pantazi, A., Moheimani, S.O.R., Pozidis, H., and Eleftheriou, E. (2008). Achieving sub-nanometer precision in a mems storage device during self-servo write process. *IEEE Transactions on Nanotechnology*, 7(5), 586 – 595.

Sebastian, A. and Salapaka, S.M. (2005). Design methodologies for robust nano-positioning. *IEEE Trans. Contr. Syst. Tech.*, 13(6), 868 – 876.

Tayebi, A., Abdul, S., Zaremba, M.B., and Ye, Y. (2008). Robust iterative learning control design: Application to a robot manipulator. *IEEE/ASME Transactions on Mechatronics*, 13(5), 608–613.